Journal of Physics: Theories and Applications E-ISSN: 2549-7324 / P-ISSN: 2549-7316
J. Phys.: Theor. Appl. Vol. 7 No. 1 (2023) 1-16 doi: 10.20961/jphystheor-appl.v7i1.64418

Spectroscopic properties and optoelectronic parameters of ternary composites incorporating poly(L-Tryptophane):P(TER-CO-TRI) and Sudan dye

Barham Kamal Rahim[1], Fahmi F. Muhammadsharif[2,1,*,ID], Salah Raza Saeed[1], Kamal Aziz Ketuly[3]

[1] Medical Physics Department, Faculty of Medicals & Applied Science, Charmo University, 46023 Chamchamal, Sulaimania, Iraq
[2] Department of Physics, Faculty of Science and Health, Koya University, 44023 Koya, Kurdistan Region, Iraq
[3] Department of Medical Chemistry, College of Medicine, University of Duhok, Duhok,, Kurdistan Region, Iraq

*Corresponding author's email: fahmi982@gmail.com
ORCID: 0000-0002-4563-9671

Received 10 August 2022, Revised 27 January 2023, Published 27 March 2023

Abstract. In this study, the spectroscopic properties and optoelectronic parameters of a ternary composite containing poly(L-Tryptophane): P(TER-CO-TRI) and Sudan dye were thoroughly investigated. Poly(L-Tryptophane) and P (TER-CO-TRI), the electron acceptor and donor, were solution processed and doped with different ratios of Sudan dye to form ternary composite systems. The FTIR technique, UV-Vis spectroscopy, and cyclic voltammetry (CV) were utilized to study the broad properties of the samples. Results showed that with the help of dye doping, the non-dispersive refractive index and energy gap of the ternary system were increased to 2.00 and decreased to 2.11 eV, respectively. The optical band gap, refractive index, dielectric constant, and optical conductivity of the samples were elaborated. The nature of the electronic transition in the studied samples was found to be a direct allowed transition, which was derived from the application of Tauc's equation. The combination of CV test and absorption spectroscopy was successfully used to determine the molecular energy levels, HOMO and LUMO of the polymer samples.

Keywords: poly(L-Tryptophane), P(TER-CO-TRI), Sudan dye, energy band gap, refractive index, dielectric constant.

1. Introduction

Optoelectronic devices have undergone a series of significant advancements over the past few decades because of the intensive study into organic semiconductors. When it comes to making low-cost organic-based gadgets, organic materials are widely recognized for their flexibility, light weight and vast surface area as well as their capacity to be tuned optically [1]. Conjugated polymers are one of the most successful and promising active layers used for organic optoelectronic devices such as organic light-

emitting diodes (OLEDs) and organic solar cells (OSCs) [2]. The contributions of organic materials in electronic devices [3] are well known, with the aforementioned properties, which are rarely seen in the inorganic materials [4]. The efficiency of organic solar cells (OSCs) has been steadily improved to reach about 16% in the single-junction based devices [5].This great achievement is in conjunction with the important developments that are continuously made in of the other organic electronic devices such as transistors, sensors, memory, diodes[6–9].

Light interaction with materials, which allows photons to be absorbed in different energy levels, has become increasingly important as a result of photovoltaic and photocatalysis activities. [10–12]. Photodiodes are p–n junction devices that can generate an electrical signal via the photovoltaic effect. Photodiodes are widely used in a variety of fields, including health care, environmental monitoring, and data transmission. [13,14]. Conventional photodiodes are operated in reverse-biased mode, which means a negative voltage is applied to the photodiode's positive terminal and vice versa. When a photodiode is exposed to light energy, it produces more free charge carriers, which promotes the reverse current that flows through the device and is transferred to the external load. Because of their high photonic response, good stability, and low binding energy of excitons (bounded electron-hole pair), inorganic semiconductors have been widely used in the majority of photodiodes [15–17]. However, organic semiconductors are far more interesting, considering their light absorption capability, flexibility, and cost effectiveness. The ability to design the electrical and optical response of thiophene rings by replacing hydrogen atoms with certain chemical groups has been confirmed [18]. To create a more balanced charge carrier among the thin solid films, it is a common practice in device manufacturing to mix electron transporting material with hole transporting material in a blend to form a bulk heterojunction active organic layer [19].

A simple solution-processed approach can be used to make a bulk heterojunction active thin film. For a cost-effective production process, this technology is ideal. For tiny organic compounds, numerous researchers have used the physical vapor deposition approach of thin-film creation [20–22]. Because of the significant characteristics of soft organic semiconductors such as low weight, absorption strength, tuneability, and solution-processability with common chemical solvents, the development of organic-based photodiodes has been the focus of interest in both academia and industry [23–25]. Stretchable organic optoelectronics is currently a promising technique for creating user-friendly integrated electronic systems comprising a variety of functional devices like thin-film transistors (TFTs), light-emitting diodes (LEDs), photodetectors, and photovoltaics. Meanwhile, ongoing research on human-skin and tissue-compatible optoelectronic devices has hinted at their potential in biomedical applications. Continuous, dependable, and accurate monitoring of physiological variables, for example, permits patients to be as mobile as they want without being restricted by their location. Patients can receive real-time self-health care at home without any constraints on their regular activities by simply transferring the extracted medical data to certified professionals for diagnostic assessment [26]. The self-powered photodiode outperformed the performance of photodiodes described in the literature in terms of sensitivity, responsivity, and detectivity under

various illumination intensities [27]. The power sources for the portable non-medical and medical devices can be provided by the mean of self-powered organic photodiodes.

However, before the full consideration of any organic material as active layer of the device, it is imperative to have a complete photo-physical information regarding the utilized organic semiconductors. More specifically, it is important to know how the absorption response of mixed semiconductors behaves in the form of binary (two component) and or ternary (three component) when they are illuminated by the light energy. The key factors of employing organic polymers in optoelectronics are absorptivity, and energy band gap [28]. As such, various conjugated polymers were simulated by researchers to explore charge transfer in the donor-acceptor systems [29]. Additionally, the use of organic semiconductors and dyes has been extensively found in the electronic devices. However, to study the organic materials and their viability for potential applications, a comprehensive study on their optoelectronic parameters, and photo-physical response is necessary. Therefore, in the current work the absorption response, optical energy gap, refractive index, dielectric constant, and optical conductivity of organic composite systems incorporating poly(L-Tryptophane):P(TER-CO-TRI) and Sudan dye are investigated.

2. Materials and methods

2.1. Synthesis of poly(triamterene-co-terephthalate) and Poly(L-tryptophan)

Triamterene (2,4,7-triamino-6-phenylpteridine,6-phenyl-2,4,7-pteridinetriamine), 99% (2.35 g) and terephthaloyl chloride flakes, 99% (2.86 g) were added into a conical flask fitted with an air condenser and blue silica drying tube. Pyridine (75 ml) was added and the solution stirred and refluxed on a hot plate for 1 h (Fig. 1). A deep orange suspension was produced and the solution was left to cool. The reaction mixture was filtered through filter paper under vacuum. The orange residue was washed with *n*-hexane: acetone: ethylacetate (70:10:20, v/v/v, 100 ml). The deep yellow solid product was dried under vacuum at RT and yielded 4.06 g.

The L-tryptophane (25.078 g) was introduced to a three-necked round bottom flask with a magnetic bar and a condenser and silica gel drying tube. Within 45 minutes at room temperature (RT), pyridine (80 ml) and thionyl chloride (20 ml, Acros Organics) were added dropwise. An extremely hot reaction occurred, resulting in a solution that turned a rich, dark red wine hue. In 250 ml of deionized water, the reaction mixture was added and a gummy product precipitated. There were repeated washings with deionized water and acetone:water (v/v) (1:1) before this solution was purified under vacuum. The solid polymeric product was dried under vacuum before being dissolved in acetone and then filtered. It was then dried under vacuum and cleaned by washing with water, dichloromethane and n-hexane: ether (9:2) and drying at 60 ^{o}C, obtaining the solid deep wine-brown product (13.232g).

2.2. Preparation of ternary composites

The polymer(L-Tryptophane) like acceptor, dopant P(TER-CO-TRI) like donor material, and Sudan dye molecular structures are shown in Figure 1. The organic materials were utilized to prepare the composite systems without additional purification. The organic materials, polymer(L-Tryptophane) and P(TER-CO-TRI), were put inside separate vials and dissolved in chloroform solvent following their stirring overnight using a magnetic stirrer. As such, solutions of polymer(L-Tryptophane) and P(TER-CO-TRI) were formed with concertation of 0.5 mg/ml. Then, different volumetric compositions of Acceptor:Donor were prepared by mixing the polymer(L-Tryptophane) solution with P(TER-CO-TRI) solution having ratios of 1:1, 1:2 1:3, 1:4 and 1:5, respectively. Finally, Area Under the Curve (UAC) of absorption profile was calculated for the samples of different donor-acceptor ratios. It was seen that AUC was highest for the 1:2 of donor:acceptor. Later on, the Acceptor: Donor(1:2) ratio was fixed at this optimum condition, followed by the addition of various Sudan dye contents into the Acceptor:Donor to yield a ternary system (1:2:1, 1:2:2, 1:2:3, 1:2:4 and 1:2:5). To investigate the properties of the samples, and estimating the optoelectronic parameters, FTIR spectroscopy, UV-Vis spectroscopy and cyclic voltammetry were used.

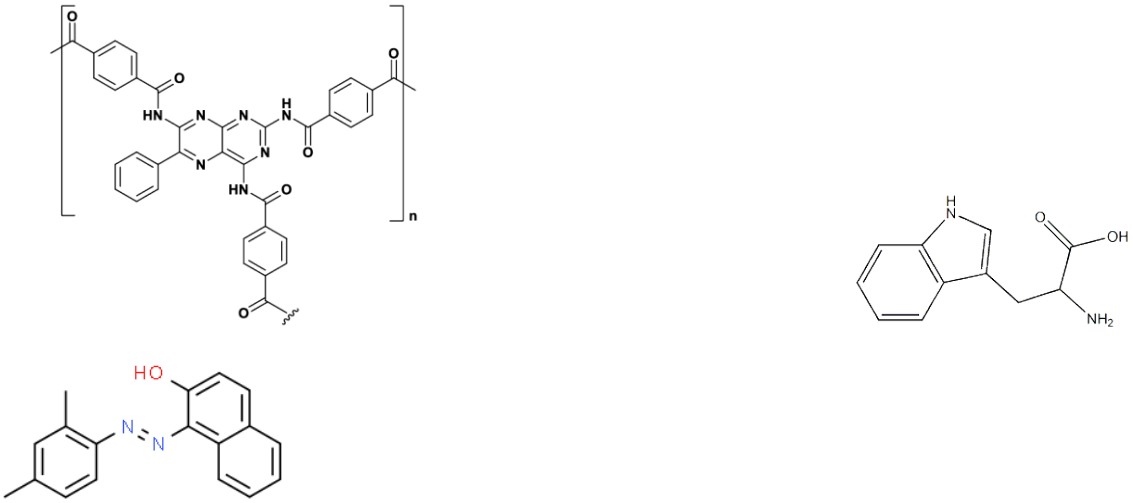

Figure 1. Molecular structure of poly(triamterene-co-terephthalate), poly(L-tryptophan) and Sudan dye (left to right).

3. Results and discussion

3.1. Spectroscopic analysis of P(TRI-CO-TER) and poly (L-Tryptophane)

FTIR spectroscopy can be used to reveal molecule structure and environment via vibrational modes, which are a feature of FTIR [30]. Figure 2(a) and 2(b) show the FTIR spectra of the synthesized polymers, P(TRI- CO -TER), and poly (L-Tryptophane) with the main IR characteristic modes. The absorption bands around 1200 to1500 cm^{-1} are assigned to C–H stretching for the aromatic rings and N–H stretching for normal vibration of the pyrrole rings, respectively [31,32]. In addition, these bands are broad and weak for P(TRI-CO-TER). This could be because the intensity of an absorption band depends on

the size of the change in dipole moment associated with the vibration and on the number of bonds responsible for the absorption. Moreover, the formation of cyclic dimers due to the presence of the carboxylic group, which consists of a proton donor and a proton acceptor group, can lead to the presence of an intermolecular hydrogen bond of the carboxylic acid with pyridine and an intramolecular hydrogen bond of the proton donor N–H with oxygen [30]. The band at 1700 cm^{-1} was attributed to the stretching vibration of the carboxylic group C=O. The out-of-plane bending mode for C–H in the spectral region from 700 to 1000 cm^{-1} could be due to the benzene ring because of the polymerization process [33]. The IR spectra as follows, λ = 1743 cm^{-1} (C=O stretch); 1327 cm^{-1}(C–N stretch) and the pheny l 1500, cm^{-1}(C=C stretch), 713 cm^{-1} (C–H bend aromatic). The IR bands at λ=3403 cm−1 (N–H stretch, pyrrole ring); 1589 cm−1 (C=O stretch); the aromatic group 1456 cm−1 (C=C stretch); 1355 cm−1 (C–N stretch) and 7410 cm−1 (C–H bend).

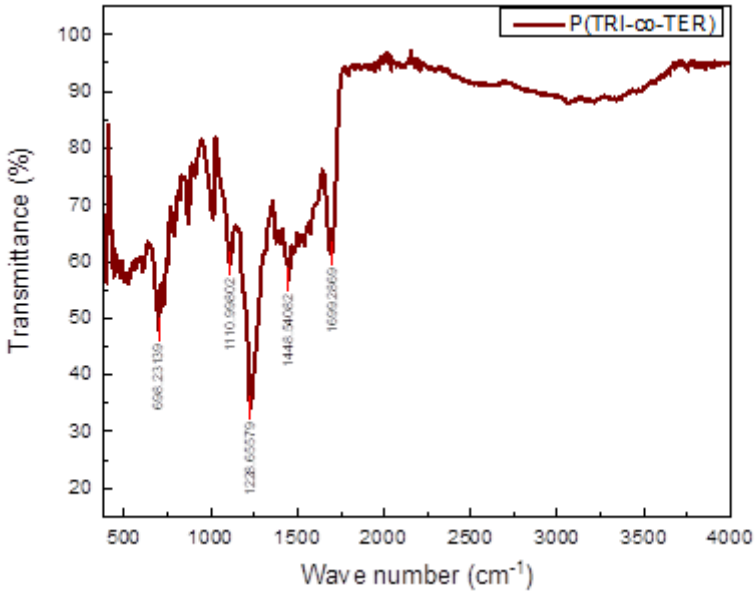

(a)

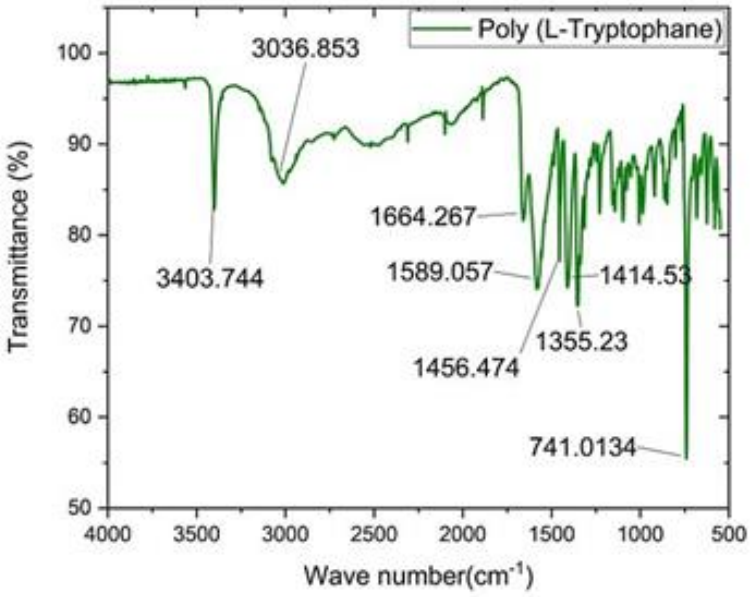

(b)

Figure 2. FTIR spectra of P(TRI-co-TER) (a) and poly (L-Tryptophane) (b).

3.2. Photophysical properties

Using UV–VIS absorption spectroscopy, the photophysical characteristics of polymer, binary, and ternary solutions were determined. It is known that the UV absorption bands can be attributed to the $\pi - \pi^*$ and $n - \pi^*$ transitions of of delocalized excitons in the polymer chain, while the visible absorption bands are attributed to intramolecular charge transfer (ICT) between electron-rich and electron-deficient moieties in the main chain [34]. The polymers' absorption coefficient spectra were calculated using the following equation [35]:

$$\boldsymbol{\alpha}=\frac{2.303A}{t} \quad (1)$$

where *t* is the thickness of the cuvette (1cm) and A is the absorbance of the studied sample. The two polymers exhibited a sharp absorption band in the UV region, and extended to the visible region. The absorption band for the acceptor poly(L-Tryptophane) was prolonged to 424 nm and the absorption band for P(TRI-co-TER) continued till 428 nm, whereas the absorption band for their mixed composite reached 430 nm. Noteworthy, upon the addition of sudan dye into the donor-acceptor system, the ternary composite structure has led to extend the absorption tail to about 593 nm. These results indicate that the transitions of delocalized excitons from $\pi - \pi^*$ and $n - \pi^*$ occur in the polymer backbones, whereas the differences in the length of the bands in the visible region for polymers are due to the degree of intramolecular charge transfer (ICT), which is related to the transition of excitons between benzenoid and quinoid rings [36].

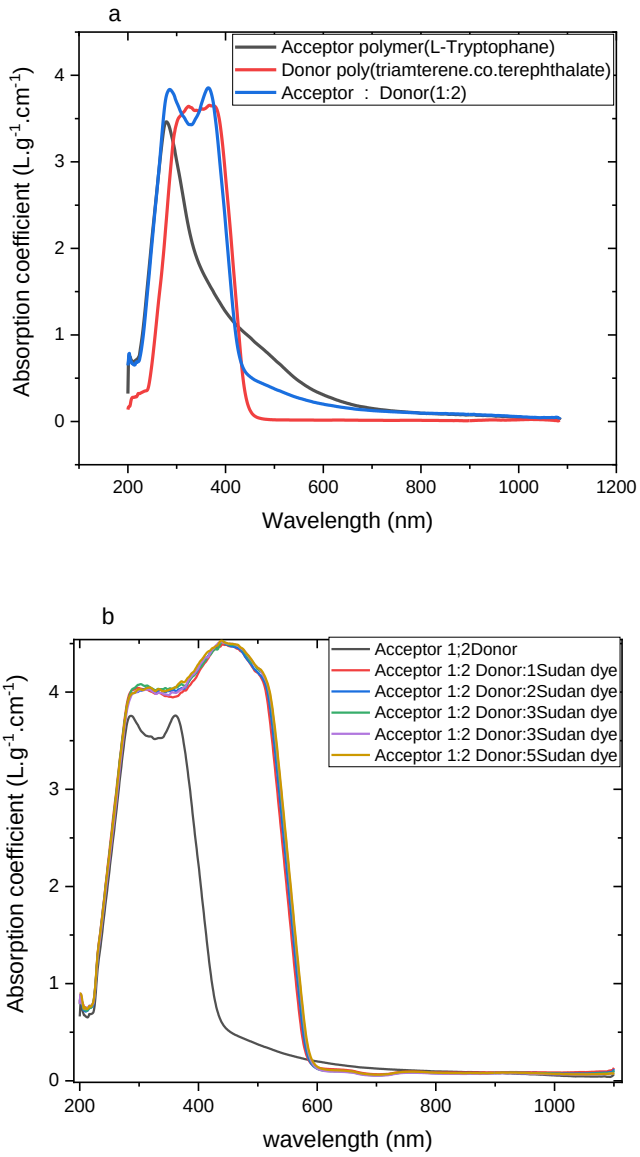

Figure 3. Absorption coefficient spectra for the two synthesized polymers and their binary system (a) along with the binary and ternary composite systems (b).

3.3. Optical energy gap and transition types

In optoelectronic applications, it is essential to quantify the optical energy gap and the type of optical transitions in conjugated polymers when evaluating the polymers' potential application. Using Tauc's equation, it is feasible to determine the optical energy gap and optical transition from the absorption spectrum. In addition, the absorption spectrum's absorption edge has been utilized to measure the optical energy gap, thereby quantifying $\boldsymbol{\lambda}_{\text{onset}}$ as follows [37]:

$$E_g = \frac{1242}{\lambda_{onset}} \tag{2}$$

Despite detecting the optical energy gap, Tauc's equations can be applied to determine the nature of the transition by taking the natural logarithm and deriving Eq. 3,

$$\alpha h\nu = \alpha_o(h\nu - Eg)^n \quad (3)$$

$$\frac{dln(\alpha h\nu)}{d(h\nu)} = \frac{n}{h\nu - Eg} \quad (4)$$

where E_g is the energy band gap, h is the Planck's constant, ν is the frequency of the wave, α_o is a constant, and the exponent n describes the type of electronic transitions [42]. When n = 2, the transition is an indirectly allowed transition, n = 3 for indirectly forbidden transitions, n = 1/2 for directly allowed transitions and n = 3/2 for directly forbidden transitions. Figure 4(a-c) shows the absorption onset of the polymers and their equivalent optical energy gaps, which were calculated from λ_{onset} (Eq. 2) and are listed in Table 1. The plots of $d\frac{dln(\alpha h\nu)}{d(h\nu)}$ versus hν for all samples are shown in Fig. 4(e) and the approximate value of hν = E_g was taken at the peak value. Hence, the estimated value of E_g was employed for plotting $ln(\alpha h\nu)$ versus ln (hν − Eg) and the value of n was determined from the slope of the curves and was found to be $\frac{1}{2}$, which shows the occurrence of a directly allowed transition between the intermolecular energy bands of the polymers. Then, the accurate values of the energy gaps were determined by plotting $(\alpha h\nu)^2$ as a function of (hν) and taking the extrapolation of the linear portion at $(\alpha h\nu)^2 = 0$. The positions of the energy gaps are depicted in Fig. 4(f) for all the polymers.

Table 1. Determined energy gap of the polymers and ternary composites from absorbance data.

Materials	$E_g^{\lambda onset}$ **(eV)**	$E_g^{Tauc's}$ **(eV)**
Donor P(TRI-co-TER)	2.70	2.97
Acceptor poly(L-Tryptophane)	2.92	3.12
Acceptor:Donor (1:2)	2.79	2.94
Acceptor:Donor:Sudan dye (1:2:3)	2.11	2.19

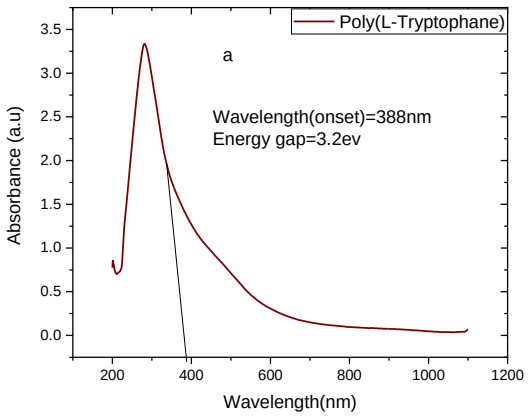

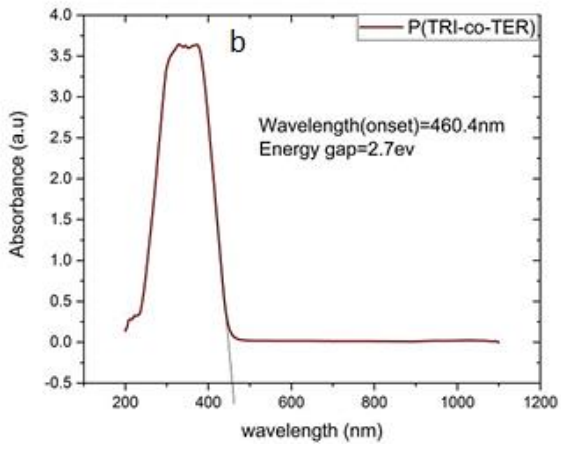

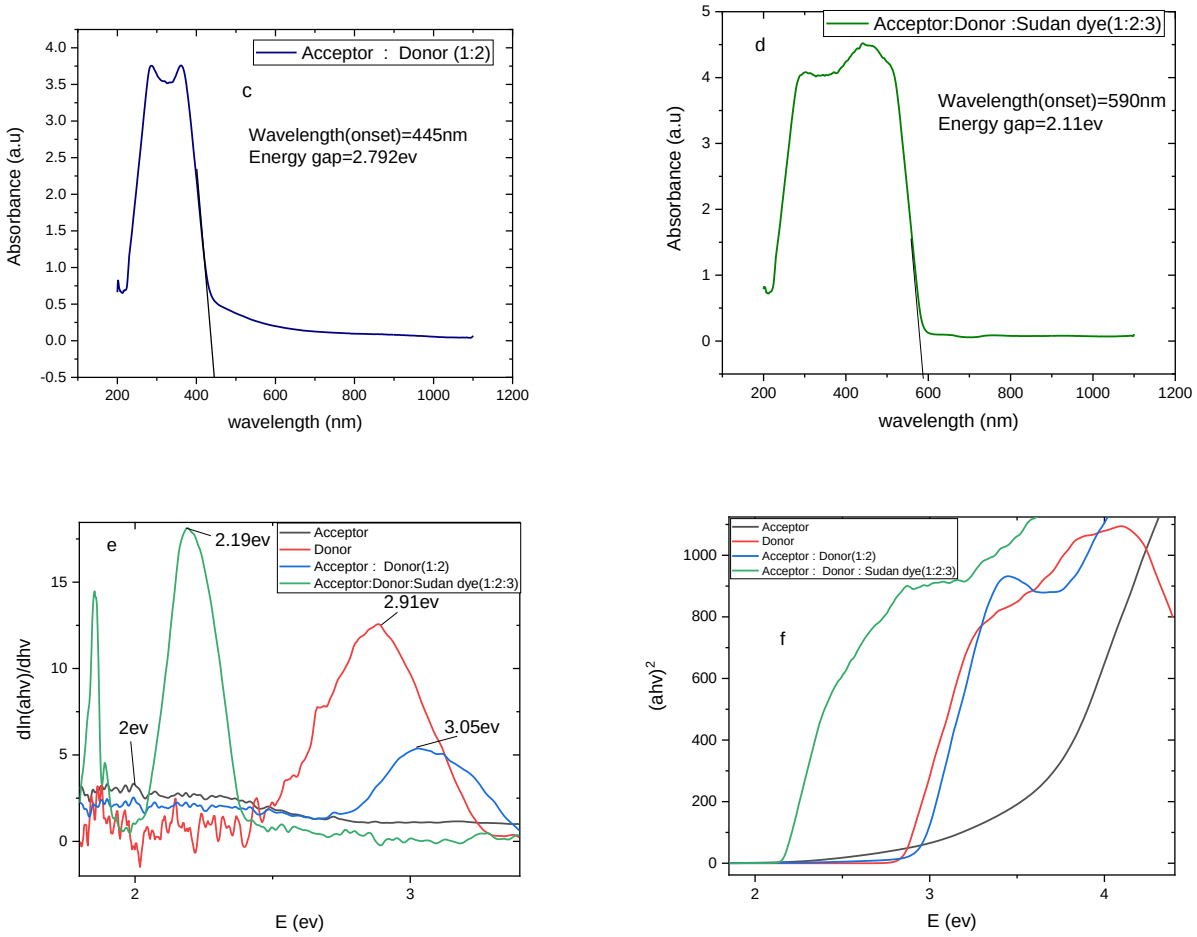

Figure 4. Absorbance spectra for the polymers, binary and ternary systems (a-d), plot of $\frac{dln(\alpha hv)}{d(hv)}$ versus hυ (e), and plot of $(\alpha hv)^2$ versus E (f).

3.4. Electrochemical properties

Charge transmission and charge collection at the active media and electrodes are just two of the many characteristics that should be taken into account while building and optimizing organic photovoltaic systems. When it comes to determining the HOMO and LUMO levels of organic materials, electrochemical studies can help. The oxidation and reduction potentials of the relevant materials can be used to determine energy levels by cyclic voltammetry (CV). Anodic and cathodic currents can be inferred from the onset potential, which is defined as the potential where holes or electrons are first injected into the HOMO and LUMO levels, respectively [39]. First, optical energy gaps were computed using Tauc's equation to get the HOMO and LUMO levels, as previously discussed. Finally, using ferrocene as a reference couple, HOMO and LUMO levels were calculated [40]:

$$E_{HOMO} = -(E(onset,oxvs.Fc+/Fc) + 5.39)\ (\text{eV}) \quad (5)$$

$$E_{LUMO} = -(E(onset,redvs.Fc+/Fc) + 5.39)\ (\text{eV}) \quad (6)$$

$$E_g^{Tauc} = E_{HOMO} - E_{LUMO} \quad (7)$$

Figure 5(a-c) depicts illustrative CVs of the two polymers versus Fc/Fc+, whereas Table 3 displays the related electrochemical parameters. The HOMO level is affected by the type of substituents (either electron-withdrawing or electron-donating species), and it can be observed that P(TRIco- TER) had a higher HOMO level than poly(L-Tryptophane). This could be because of the indole N–H group. In addition, P(TRI-co-TER) has comparable molecular energy levels, and the LUMO level of P(TRI-co-TER) is 2.92 eV, whereas the LUMO level of poly(L-Tryptophane) is 2.87ev (estimated from E_{ox} and E_g due to the faint observation of Ered on the CV plot) (Table 2) [41].

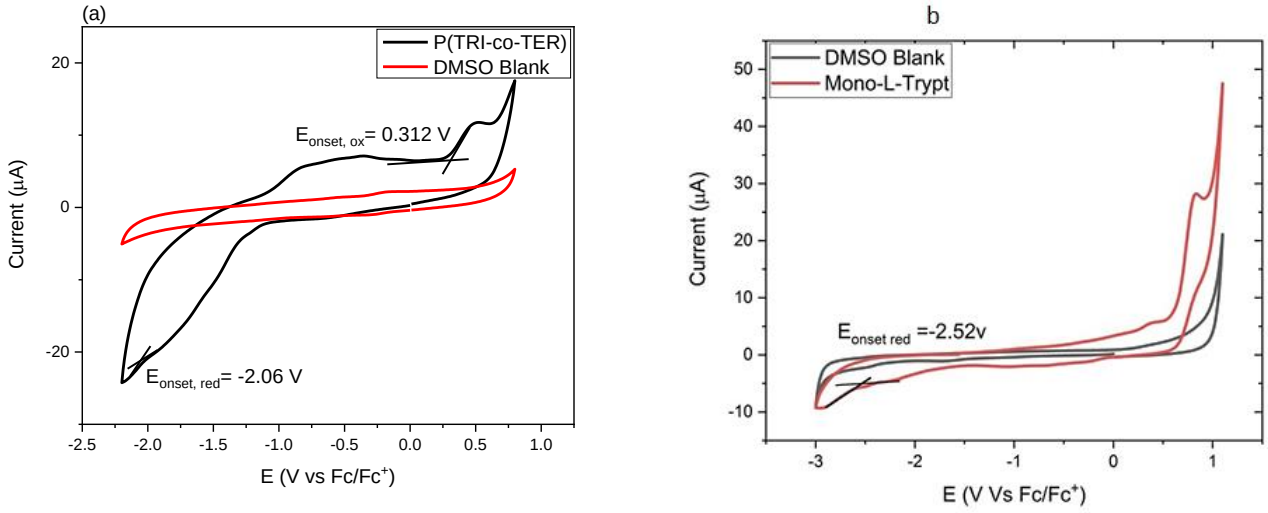

Figure 5. The Cyclic Voltammetry (CV) spectra for all synthesized polymers. The irreversible oxidative processes observed in the CVs are likely due to the oxidation of adventitious water in the DMSO solvent

Table 2. Electrochemical and optical data for all synthesized polymers

Polymer	$E_{onset,ox}$ ***(V)***	$E_{onset,red}$ ***(V)***	E_{HOMO} ***(eV)***	E_{LUMO} ***(eV)***	E_g ***(eV)***
P(TRIco- TER)	0.312	-1.24	-5.70	-2.78	2.92
poly(L-Tryptophane)	NA	-2.52	-5.39	-2.87	2.52

3.5. Optical constants

Before applying the materials in photovoltaic devices, optical constants such as refractive index and extinction coefficient and their derivative parameters such as dielectric constant and optical conductivity must be addressed. Examining the refractive index reveals the electromagnetic wave's propagation within the material and the change

in speed inside the substance relative to the vacuum. In addition, it is a complex variable whose imaginary component represents the amount of energy lost due to the medium and is known as the extinction coefficient. Using Equations 8 and 9, absorbance measurements were utilized to compute the refractive index (n) and extinction coefficient (k) [42].

$$n = \frac{-2(R+1)-\sqrt{4K2}R2+16R-4K2}{2(R-1)} \quad (8)$$

$$k=\frac{\alpha\lambda}{4\pi} \quad (9)$$

where $\boldsymbol{\alpha}$ is the absorption coefficient and R is the reflectance. They were calculated using Eq. 4 and the following equation: R = 1 − T − A, where A is absorbance and T is transmittance and estimated from $T = 10^{-A}$. Figure 6 and 7 show the variation of refractive index and extinction coefficient, respectively as a function of wavelength from 200 to 1100 nm. Results show that the P(TRI-co-TER) and poly(L-Tryptophane) have a wider dispersion region between 230 and 480 nm and 249 nm to 431 nm than that for this mixed Acceptor: Donor(1:2), which was extended from 281 nm to 427 nm and for the Acceptor:Donor:dye (1:2:3) from 209 nm to 600 nm. In addition, the extinction coefficient (k) represents the photon loss caused by scattering and absorption within the medium. Notably, the variance of (k) is nearly equivalent to the corresponding absorption coefficient (Eq. 9) [43]. All samples exhibit a UV absorption peak that extends to varying degrees into the visible spectrum. The optical dielectric constant (ε) is a frequency-dependent quantity that represents the material's electrical reaction to an incident photon. In the meantime, the dielectric constant is a complex function whose real component corresponds to polarization under the influence of an electromagnetic field, whilst its imaginary part represents optical loss and is given by the following equations [44].

$$\varepsilon=\varepsilon_1+i\varepsilon_2 \quad (10)$$

$$\varepsilon_1=n^2-k^2 \quad (11)$$

$$\varepsilon_2=2nk \quad (12)$$

$$\tan\delta=\frac{\varepsilon 2}{\varepsilon 1} \quad (13)$$

where 1 represents the real portion of the dielectric constant and 2 represents the imaginary portion. Figures 6(a) and 6(b) illustrate the variation of the optical dielectric constant vs wavelength from 200 to 1100 nm. Due to the tiny value of k, the real portion of the spectrum of the optical dielectric constant reflects the refractive index, but the imaginary portion is mostly based on the absorption coefficient (see Eqs. 9, 11 and 12). demonstrate that the poly(L-Tryptophane) and P(TRI-co-TER) concentrations are greater for this mixed Acceptor: Donor (1:2) and this mixed Acceptor: dye Sudan (1:2:3)

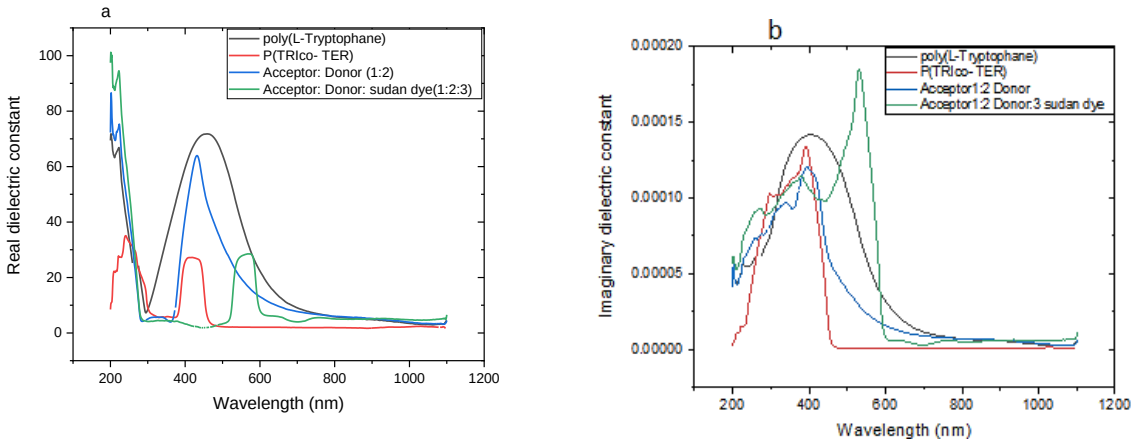

Figure 6. Dielectric constant spectra for the polymers, binary and ternary samples; (a) real part, and (b) Imaginary part

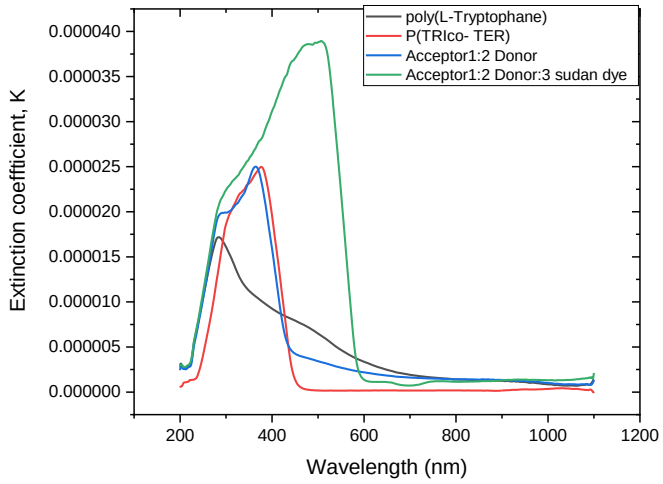

Figure 7. The extinction coefficient spectra of the polymers and composite systems.

Figure 8 shows the refractive index of the studied solution in the wavelength range from 200 to 1000 nm. It was observed that refractive index follows an anomalous dispersion in the UV and near Vis wavelength (absorption region) and a non-dispersive response in the far Vis and IR wavelengths (transparent region). The non-dispersive/flattened property of refractive index is called infinite refractive index (n_∞). Its value for the investigated solution is shown in Table 2. According to the results, the refractive index of P(TRI-co-TER) (n = 1.39) and poly(L-Tryptophane (n = 1.95) is lower than that of the dopant mixed Acceptor: Donor(1:2) (n = 1.99) and lower than that of the dopant mixed Acceptor1:2 Donor and mixed Acceptor: Donor: sudan dye(1:2:3) (n = 2), which is consistent with those reported in [45]. Intriguingly, poly(L-Tryptophane) (n = 1.95) dopant can raise the refractive index of P(TRI-co-TER) from (n = 1.39) to (n = 1.99) and to (n = 2) in the Acceptor: Donor(1:2) system, in comparison to the Acceptor: Donor: sudan dye (1:2:3) system. Notably, the peak of the refractive index shifts to the blue as

the poly(L-tryptophan) concentration rises, reflecting the expectation that the energy gap will reduce proportionally.

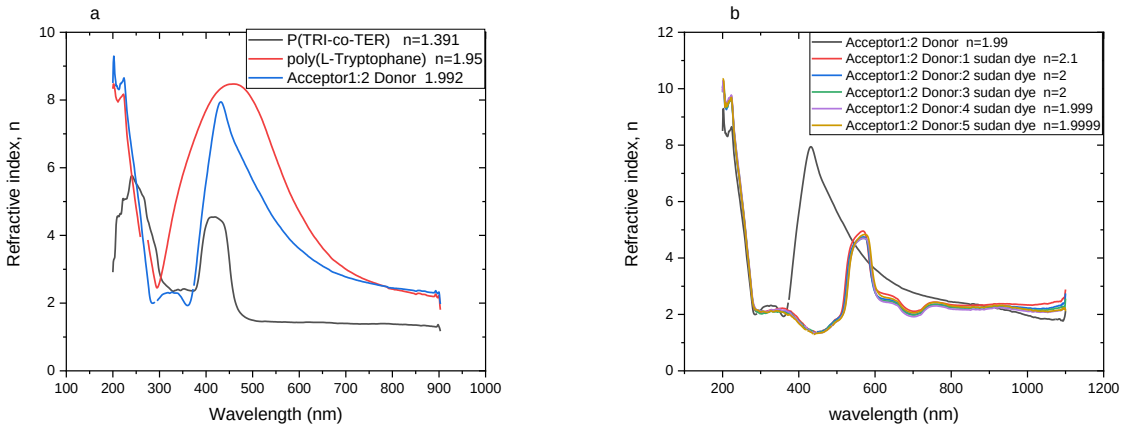

Figure 8. Refractive index spectra of the pristine of the polymers and composite systems.

Table 3. The studied optoelectronic parameters of the poly(L-Tryptophane), P(TRI-co-TER), Acceptor: Donor (1:2) and Acceptor: Donor:sudan dye (1:2:3) by solution.

solution	***n***	ε_r	$\sigma_r \times 10^{-4}$ ***(S cm^{-1})***
Donor P(TRI-co-TER)	1.39	2.77	2.51
Acceptor poly(L-Tryptophane)	1.95	1.95	3.40
Acceptor1:2 Donor	1.99	2.82	2.61
Acceptor1:2 Donor: 3Sudan dye	2.00	2.63	2.30

Furthermore, the real and imaginary components of optical con ductivity ($\sigma^* = \sigma r + i\sigma i$) can be investigated by means of the following formula:

$$\sigma_r = \omega \varepsilon_o \varepsilon_i \quad (14)$$

$$\sigma_i = \omega \varepsilon_o \varepsilon_r \quad (15)$$

Where σ_r is the real optical conductivity, σ_i is the imaginary optical conductivity, ω is the angular frequency and ε_o is free space permittivity (8.85×10^{-12} F m^{-1}). Figure 9(a) shows the σ_r spectra of the investigated Acceptor: Donor (1:2) and Acceptor: Donor: sudan dye (1:2:3). One can notice from the figure that the value of real optical conductivity is getting constant/non-dispersive at the high wavelengths. The graphs reveal that the value of real optical conductivity becomes constant and non-dispersive at longer wavelengths. This demonstrates that the variation in optical conductivity is directly proportional to the variation in the number of excited electrons caused by the solutions' absorption of photon energy. Therefore, the increase in UV-region optical absorption of the examined solutions is a result of enhanced optical conductivity, and vice versa. Figure 9(b) depicts the imaginary optical conductivity of the solution of Acceptor:Donor (1:2) and Acceptor:Donor:sudan dye (1:2:3). Results indicate that σi decreases exponentially with increasing wavelength. Doping the Acceptor:Donor (1:2) with poly(L-Tryptophane) results in a significant drop in σi notably in the UV spectral region. However, the

Acceptor: Donor: Sudan Dye (1:2:3) exhibits a greater σi than the other samples, which can be attributed to the enhanced π-π stacking and decreased band gap energy. The dissipation factor for the ternary system is greater than that of the other samples, as seen in Figure 10.

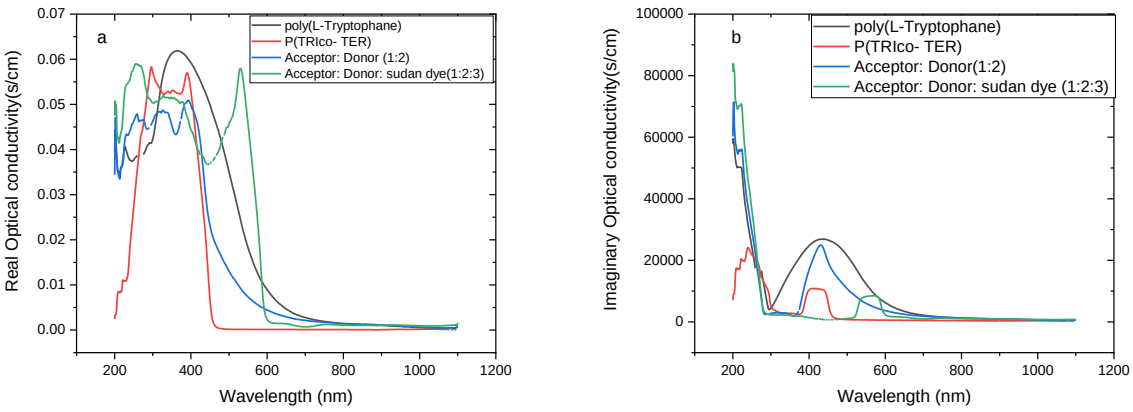

Figure 9. Optical conductivity spectra for the polymers and composite systems; (**a) r**eal part, and (**b**) imaginary part

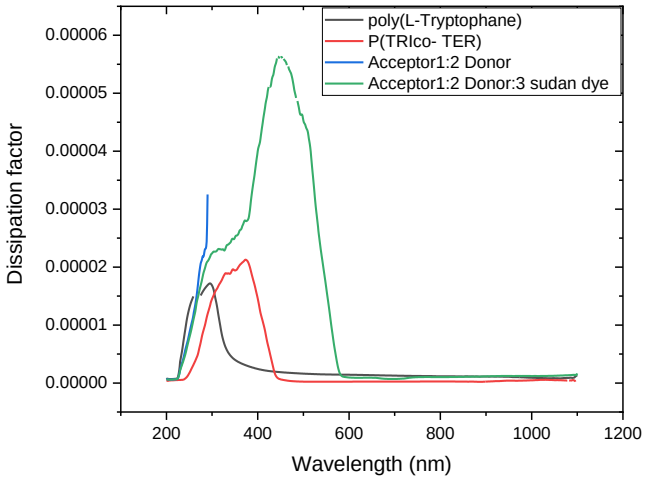

Figure 10. Dielectric lost tangent (dissipation factor) spectra for polymers and composite systems.

4. Conclusions

A thorough examination of the spectroscopic characteristics and optoelectronic parameters of a ternary composite containing poly(L-Tryptophane):P(TER-CO-TRI) and Sudan dye was accomplished. Using FTIR, UV-Vis spectroscopy, and cyclic voltammetry (CV), the optical band gap, refractive index, dielectric constant, and optical conductivity of the materials were investigated. The non-dispersive refractive index and energy gap of the ternary system were enhanced to 2.00 and lowered to 2.11 eV, respectively, with the aid of dye doping. The application of Tauc's equation revealed that the nature of the electronic transition in the investigated samples was a direct permitted

transition. Using a combination of the CV test and absorption spectroscopy, the HOMO and LUMO molecular energy levels of polymer samples were successfully determined.

Statements and Declarations

Competing Interests: The authors declare that there is no conflict of interest regarding the publication of this paper.

References

Y. Peng, B. Lu, and S. Chen, Advanced Materials **30**, 1870370 (2018).

C. Zhan, G. Yu, Y. Lu, L. Wang, E. Wujcik, and S. Wei, Journal of Materials Chemistry C **5**, 1569 (2017).

N. J. Vickers, Current Biology **27**, R713 (2017).

M. Sajid, M. Zubair, Y. Hoi, and D. K. Na, Journal of Materials Science: Materials in Electronics **26**, 7192 (2015).

B. Fan, D. Zhang, M. Li, W. Zhong, Z. Zeng, and L. Ying, (2019).

Q. Y. Ang, M. H. Zolkeflay, and S. C. Low, Applied Surface Science **369**, 326 (2016).

J. Jayabharathi, V. Thanikachalam, and P. Ramanathan, SPECTROCHIMICA ACTA PART A: MOLECULAR AND BIOMOLECULAR SPECTROSCOPY **150**, 886 (2015).

H. G. Lazim, K. I. Ajeel, and H. A. Bdran, SPECTROCHIMICA ACTA PART A: MOLECULAR AND BIOMOLECULAR SPECTROSCOPY (2015).

M. A. M. Sarjidan, S. H. Basri, M. S. Zaini, and W. H. A. B. D. Majid, **38**, 1 (2015).

S. Zinatloo-ajabshir, M. Sadat, and M. Salavati-niasari, Composites Part B **167**, 643 (2019).

F. Razi, S. Zinatloo-ajabshir, and M. Salavati-niasari, Journal of Molecular Liquids (2016).

S. Zinatloo-ajabshir, S. Mortazavi-derazkola, and M. Salavati-niasari, **42**, 171 (2018).

T. Alzoubi, H. Qutaish, E. Al-shawwa, and S. Hamzawy, Opt Mater (Amst) **77**, 226 (2018).

S. Alamdari, M. Sasani, H. Afarideh, and A. Mohammadi, Opt Mater (Amst) **92**, 243 (2019).

Q. Xu, L. Cheng, L. Meng, Z. Wang, S. Bai, X. Tian, X. Jia, and Y. Qin, (2019).

H. Wang, P. Sun, S. Cong, J. Wu, L. Gao, Y. Wang, X. Dai, Q. Yi, and G. Zou, Nanoscale Research Letters 1 (2016).

D. Guo, Y. Su, H. Shi, P. Li, N. Zhao, J. Ye, S. Wang, A. Liu, Z. Chen, C. Li, and W. Tang, ACS Nano **12**, 12827 (2018).

X. Liu and M. Knupfer, **595**, 165 (2005).

R. D. J. Vuuren, A. Armin, A. K. Pandey, P. L. Burn, and P. Meredith, (2016).

Q. Dai and X. Q. Zhang, **18**, 11821 (2010).

D. A. I. Qian, Z. H. U. Lu, S. U. N. Jian, Z. Xiqing, and W. Yongsheng, **55**, 1551 (2012).

D. Ray, K. L. Narasimhan, D. Ray, and K. L. Narasimhan, **093516**, 1 (2007).

L. Zhang, T. Yang, L. Shen, Y. Fang, L. Dang, and N. Zhou, 6496 (2015).

A. Omidvar, Materials Chemistry and Physics (2017).

F. F. Muhammad, M. Y. Yahya, F. Aziz, M. A. Rasheed, and K. Sulaiman, Journal of Materials Science: Materials in Electronics **28**, 14777 (2017).

H. Lee, Z. Jiang, T. Yokota, K. Fukuda, S. Park, and T. Someya, Materials Science and Engineering R: Reports **146**, 100631 (2021).

H. Alzahrani, K. Sulaiman, F. F. Muhammadsharif, S. M. Abdullah, A. Y. Mahmoud, R. R. Bahabry, and S. F. Ab Sani, Journal of Materials Science: Materials in Electronics **32**, 14801 (2021).

D. Kajiya, T. Koganezawa, and K. I. Saitow, AIP Advances **5**, (2015).

P. Song, Y. Li, F. Ma, T. Pullerits, and M. Sun, Journal of Physical Chemistry C **117**, 15879 (2013).

D. Y. Duygu, T. Baykal, Đ. Açikgöz, and K. Yildiz, **22**, 117 (2009).

S. Wojtulewski and M. Kalinowska, **993**, 448 (2011).

L. Schmidt, J. Jonathan, R. Arias, B. Pedroso, M. De Fátima, V. Marques, and S. Neves, Integrative Medicine Research **9**, 7975 (2020).

E. D. Configuration, (2017).

Y. Huang, F. Wu, M. Zhang, S. Mei, P. Shen, and S. Tan, Dyes and Pigments **115**, 58 (2015).

H. M. Alsoghier, M. A. Selim, H. M. A. Salman, H. M. Rageh, M. A. Santos, S. A. Ibrahim, M. Dongol, T. Soga, and A. A. Abuelwafa, Journal of Molecular Structure (2018).

H. Naja and A. Bahari, **217**, 19 (2016).

L. Leonat, G. Sb, I. V. Br, and I. Cyclic, **75**, (2013).

P. Taylor, E. A. Davis, and N. F. Mott, 37 (2006).

T. Johansson, W. Mammo, M. Svensson, R. Andersson, and O. Ingana, 1316 (2003).

C. M. Cardona, W. Li, A. E. Kaifer, D. Stockdale, and G. C. Bazan, 2367 (2011).

T. Ameri, J. Bloking, T. Ameri, P. Khoram, J. Min, and C. J. Brabec, (n.d.).

F. Fariq, M. Shujahadeen, and S. A. Hussein, 521 (2015).

S. B. Aziz, O. Gh, and A. Ahang, Journal of Materials Science: Materials in Electronics **0**, 0 (2017).

P. O. Amin, A. J. Kadhim, M. A. Ameen, and R. T. Abdulwahid, Journal of Materials Science: Materials in Electronics **0**, 0 (2018).

W. Holzer, A. Penzkofer, and H. H. Hörhold, Synthetic Metals **113**, 281 (2000).